ELSEVIER

Physica D 113 (1998) 346–365

PHYSICA D

Wave propagation in linear and nonlinear structures

E. Lidorikis [a], K. Busch [a,b], Qiming Li [a], C.T. Chan [a,c], C.M. Soukoulis [a,*]

[a] *Ames Laboratory-USDOE and Department of Physics and Astronomy, Iowa State University, Ames, IA 50011, USA*

[b] *Institüt für Theorie der Kondensierten Materie, Universität Karlsruhe, 76128, Karlsruhe, Germany*

[c] *Department of Physics, The Hong Kong University of Science and Technology, Clear Water Bay, Kowloon, Hong Kong*

Abstract

We consider the general problem of electromagnetic wave propagation through a one-dimensional system consisting of a nonlinear medium sandwiched between two linear structures. Special emphasis is given to systems where the latter comprise Bragg-reflectors. We obtain an exact expression for the nonlinear response of such dielectric superlattices when the nonlinear impurity is very thin, or in the δ-function limit. We find that both the switching-up and switching-down intensities of the bistable response can be made very low, when the frequency of the incident wave matches that of the impurity mode of the structure. Numerical results for a nonlinear layer of finite width display qualitatively similar behavior, thus confirming the usefulness of the simpler δ-function model. In addition, an analytical solution for the resonance states of an infinitely extended finite width superlattice with a finite width nonlinear impurity is presented. Finally, we investigate the adequacy of the Kronig–Penney δ-function model in describing the electromagnetic wave propagation in periodic structures consistent of thin layers of materials with an intensity-dependent dielectric constant. Copyright © 1998 Elsevier Science B.V.

1. Introduction

Dielectric materials with an intensity-dependent dielectric constant are well known for their complex response to radiation. Exciting features such as bistability, multistability, optical limiting, etc. have been predicted theoretically [1,2] and observed experimentally [3–5]. Promising future applications include optical switches and transistors, pulse shapers as well as memory elements. Already quite simple structures like the traditional Fabry–Pérot etlons [3] or multilayered structures of alternating nonlinear dielectric materials [6] exhibit such a behavior. The common characteristic of all nonlinear optical devices is the feedback mechanism, necessary to enhance the nonlinear effects. Crudely speaking, there exist two types of realizations: In the case of a "localized" feedback structure a homogeneous nonlinear medium is placed between two reflectors (mirrors [3,7] or Bragg-reflectors [8]), while "distributed" feedback mechanisms are realized through a periodic modulation of the linear part of the nonlinear materials' refractive index [1]. Similar studies have been done for the electronic response in a one-dimensional nonlinear lattice [9–11], as well as for a linear lattice with nonlinear impurities [12].

* Corresponding author.

PII S0167-2789(97)00289-3

The linear (or low intensity) properties of the feedback mechanism are important for the nonlinear response of the device. For instance, a distributed feedback structure gives a photonic band gap [13,14], where certain modes are forbidden while others propagate freely. For frequencies inside the transmission band, bistability results from a modulation of transmission by an intensity dependent phase shift. For frequencies inside the stop gap of the linear system, bistability and resonance transmission is achieved via gap soliton formation [15,16].

However, nonlinear media are usualy quite lossy and, thus it is important to find ways of keeping the amount of nonlinear material small while still retaining sizable nonlinear effects. Furthermore, the successful use of optical switches depends crucially on a low threshold, i.e. low "switching" intensities. The above considerations lead to the question whether a single nonlinear layer, suitably supplied with a feedback mechanism, may be sufficient for optical switching devices. In this paper we present the results of our investigation of this and several related problems. The paper is divided into two parts: The first part deals with the general case of a "localized" feedback structure when the nonlinear layer is very thin, or in the δ-function approximation. We will give arguments why a system consistent of a nonlinear layer sandwiched between Bragg-reflectors may be considered the most efficient "localized" feedback structure, as well as which system's parameters give the lowest bistability threshold. We also demonstrate the usefulness of the δ-function approximation by comparing with numerical results for a nonlinear layer of finite width. However, a finite nonlinear layer always exhibits multistability This is illustrated in the second part of this paper, where we present an analytical solution for the resonance states of an infinite superlattice with a finite width nonlinear impurity layer. These are modulated band gap impurity modes and correspond to the transmission resonances in the multistable input vs. output diagram. Finally, in the third part, we extend the investigation on the usefulness of the δ-function approximation by comparing the results derived from the Kronig–Penny δ-function model with direct numerical solutions of wave propagation in nonlinear superlattices of finite thickness. We find that the Kronig–Penney δ-function model captures most of the essential features of the nonlinear response in superlattice structures. The global transmission diagrams from the two methods are in excellent agreement with each other. However, some disagreement does exist, most significantly below the bottom of the transmission band. This difference is entirely due to the rigidness of the band edge in the Kronig–Penney δ-function model, an unphysical feature that affects the conclusion regarding the existence of gap solitons when the Kerr nonlinearity is positive.

2. Very thin nonlinear layer

Many features of wave propagation through one-dimensional nonlinear structures can most conveniently be investigated and understood within a nonlinear Kronig–Penney δ-function model [17]. Although discrepancies with the more realistic finite width models do exist, it has been demonstrated that the δ-function model captures most of the essential features of nonlinear response to radiation [18]. In this section we consider a very thin nonlinear layer centered at the origin whose dielectric function $\epsilon(x)$ is intensity dependent:

$$\epsilon(x) \approx \epsilon_0(1 + \lambda|E(x)|^2)\delta(x). \tag{1}$$

Here ϵ_0 is defined as the limit $n^2 d \to \epsilon_0$ for $n \to \infty$, $d \to 0$, of a finite width layer of extent d and index of refraction n. $\epsilon_0\lambda$ is the corresponding nonlinear Kerr-coefficient.

We first discuss the problem of a single nonlinear δ-function. More insight is obtained from a general discussion of a δ-function nonlinear layer sandwiched between two linear structures. It will be shown that the equation relating input and output intensities has the same form as for a single nonlinear δ-function except for a parameter renormalization. Also, a very useful phase diagram for the onset of bistability in terms of the linear properties of the system will be derived. From this it follows that the most interesting physics appears when the linear structures on the two sides

of the nonlinear layer are identical Bragg-reflectors. Assuming the latter to consist of very thin layers, we arrive at a remarkably simple but very rich result for the input–output intensity relation.

2.1. Single nonlinear δ-function

We consider the problem of electromagnetic wave propagation through a single δ-function with an intensity dependent dielectric strength as given by Eq. (1). This is schematically depicted in Fig. 1. Our interest lies in the steady state response of the system. Let a plane wave $E_0 e^{-ikx}$ with wave number $k = \omega/c$ be incident from the right. This gives rise to a reflected wave, $E_r e^{ikx}$, as well as to a transmitted wave, $E_t e^{-ikx}$. Solving the Maxwell equation with a single nonlinear δ-function layer at $x = 0$ will yield a relationship between the incident and transmitted intensity, $Y = |E_0|^2$ and $X = |E_t|^2$, respectively:

$$Y = X[1 + \tau(1 + \lambda X)^2], \tag{2}$$

where $\tau = \epsilon_0^2 k^2/4$ is related to the transmission coefficient $|T_0|^2$ of the corresponding linear system, $\tau = (1 - |T_0|^2)/|T_0|^2$. The system will exhibit bistability if we can have more than one output for a given input. This will be true if Y is a nonmonotonic function of X. We find a physical solution for $dY/dX = 0$ only for $\lambda < 0$ and $\tau > 3$:

$$X_\pm = \frac{2 \pm \sqrt{1 - 3/\tau}}{3|\lambda|}. \tag{3}$$

The absence of bistability for a positive Kerr-coefficient is one of the artifacts of the δ-function approximation. We will see later that this restriction is lifted, once the nonlinear δ-function is placed between two linear systems with nonzero reflection coefficients.

The nonlinear response of such a system with negative λ is shown in the input vs. output diagram in Fig. 2(a) for various values of τ and λ. The switching-up and switching-down intensities are given by $Y_\pm = Y(X_\mp)$, respectively. For $\tau = 3$ and $\lambda < 0$ we have the onset of bistability at $Y_+ = Y_- = 8/(9|\lambda|)$. As τ gets larger, $Y_- \to 1/|\lambda|$ while $Y_+ \sim \tau/|\lambda|$. Note that for $Y = X = 1/|\lambda|$ we have resonance transmission. Thus for large τ (or equivelantly for low linear transmission) the switching-down intensity and the resonance intensity are the same. Clearly, the larger the $|\lambda|$, the smaller the switching intensities.

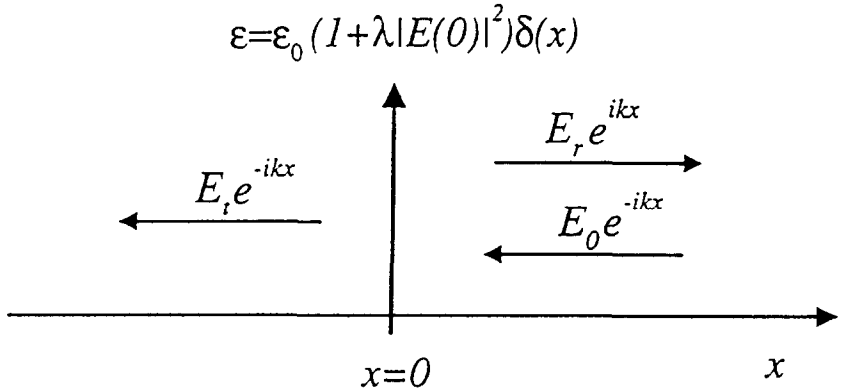

Fig. 1. Geometry considered in this section. A plane wave of amplitude E_0 strikes a nonlinear δ-function, giving rise to a reflected and a transmitted wave.

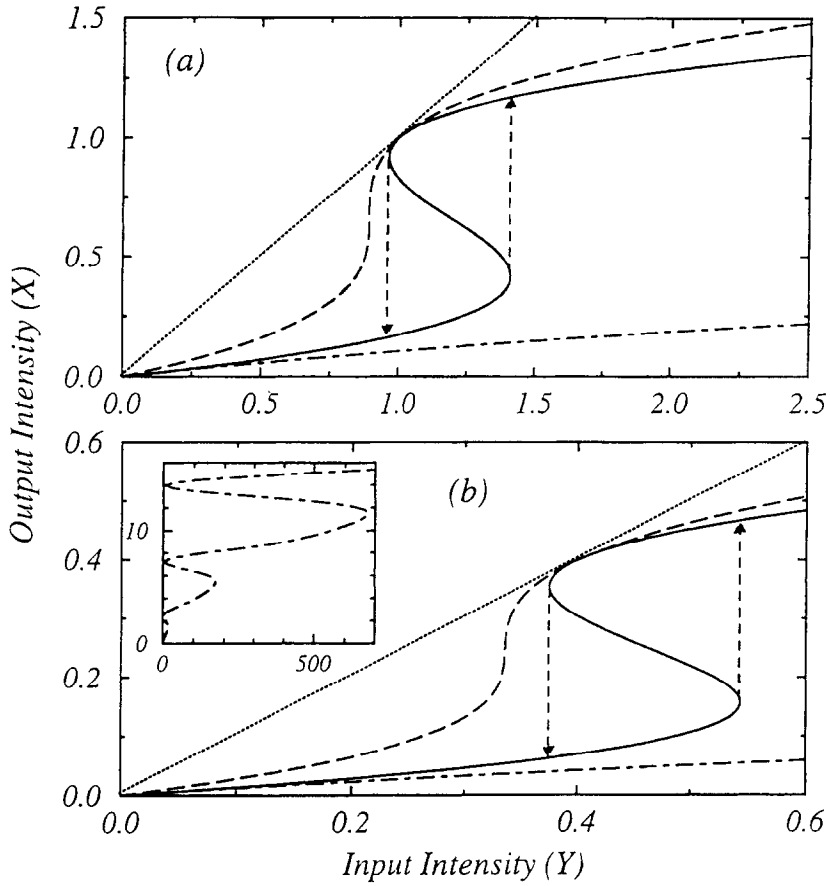

Fig. 2. Transmitted intensity vs. incident intensity for (a) a nonlinear δ-function and (b) a nonlinear dielectric slab of width $d = 0.6\lambda_f$. In both cases, the dahsed line corresponds to $\lambda = -1$ and linear transmission $T_0 = 0.25$, the solid line to $\lambda = -1$ and linear transmission $T_0 = 0.125$, and the dot–dashed line to $\lambda = +1$ and linear transmission $T_0 = 0.125$. Note that the bistability onset happens for the same system parameters. However, for large intensities the finite layer system with $\lambda > 0$ will always display multistable behavior (inset graph in (b), for the same parameters: $\lambda = +1$, $T_0 = 0.125$). The dotted line is the total transmission relation $Y = X$.

Note further, that the resonance transmission intensities $Y = X = 1/|\lambda|$ correspond to $\langle dn_{\text{eff}}^2 \rangle \equiv \epsilon_0 = 0$, i.e. the δ-function effectively disappears altogether, leading to total transmission. On the other hand, for a finite width linear layer with dielectric constant $\epsilon = n^2$, the condition for resonance transmission is $2d = m\lambda_f$, where d is the width of the layer and $m\lambda_f$ is an integer multiple of the wavelength inside the dielectric material ($\lambda_f = 2\pi c/n\omega$) [6]. If we incorporate a nonlinear coefficient in the dielectric constant ($\epsilon(x) = n^2(1 + \lambda|E(x)|^2)$), then for suitable choices of the parameters we can have bistability (and even multistability) for both negative and positive Kerr medium. For example, if $2d < \lambda_f$ and $\lambda > 0$, then effectively the dielectric constant will get larger, yielding a smaller average effective wavelength $\langle \lambda_f \rangle$. For some intensity we should expect the resonance condition to be "effectively" satisfied, and so to get a transmission resonance. Higher-order resonances are also expected giving rise to multistability. For a nagative Kerr-coefficient and $2d < \lambda_f$ we should not expect bistability, as correctly pointed out by Chen and Mills [2], unless we allow the unphysical situation at which the intensities become large enough to make $\langle n_{\text{eff}}^2 \rangle \leq 1$. Only then we would get bistability, and this would be the exact correspondence to the δ-function case. For a positive Kerr-coefficient, however, bistability should always be expected (although some times only at unrealistically high

intensities), a feature that is absent in the δ-function model. In Fig. 2(b) we show the transmission diagram for a finite width dielectric slab for $d = 0.6\lambda_f$ and various values of linear transmission coefficient and nonlinear Kerr-coefficient. Although this is not the exact analog of Fig. 2(a), it is remarkable that both models show similar dependence on their linear transmission properties. We also find that for larger intensities the negative nonlinear medium does not exhibit multistability, while a positive nonlinear medium will always exhibit multistability, as can be seen in the inset graph in Fig. 2(b).

The unphysical condition for resonance transmission in the single nonlinear δ-function case can be lifted if we sandwich the δ-function between two linear systems. Bistability will then occur as a result of the intensity dependent phase shift that the δ-function will introduce between the two linear systems, which will alter their transmission characteristics. As we will see in the next section, this arrangement is also optimal for obtaining lower switching intensities.

2.2. *Nonlinear δ-function sandwiched between two linear systems*

Let us now consider a more general geometry as shown in Fig. 3, where a nonlinear δ-function is sandwiched between two linear systems, characterized by the reflection and transmission amplitudes, r_i and t_i $(i = 1, 2)$, respectively. Generally, a linear system is described by the transmission matrix relating the incoming field amplitudes A and D from the left and the right to the outgoing field amplitudes B and C,

$$\begin{pmatrix} C \\ D \end{pmatrix} = \begin{pmatrix} 1/t^* & -r/t \\ -(r/t)^* & 1/t \end{pmatrix} \begin{pmatrix} A \\ B \end{pmatrix}. \tag{4}$$

Just as before, we assume this composed object to be illuminated from the right by a plane wave with amplitude E_0. The corresponding reflected and transmitted wave amplitudes are denoted by E_r and E_t, respectively. Then the relation between the output intensity $Y = |E_t|^2$ and the input intensity $X = |E_0|^2$ can be obtained straightforwardly by properly matching the values of the fields at the origin:

$$Y = X[\gamma + \tau'(1 + \lambda' X)^2]. \tag{5}$$

Note that Eq. (5) has exactly the same structure as Eq. (2). Thus we have shown that the introduction of the linear structures leads to a renormalization of the quantities in Eq. (2): $1 \to \gamma$, $\tau \to \tau'$ and $\lambda \to \lambda'$. The quantities γ, τ'

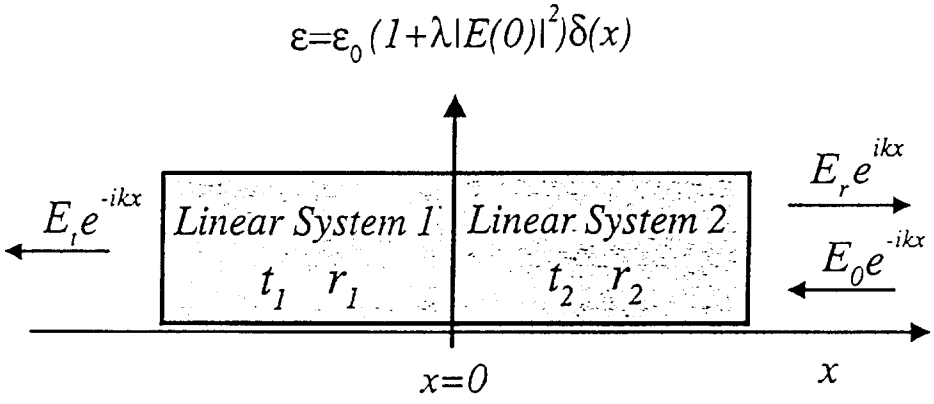

Fig. 3. The general geometry considered in this section. A nonlinear δ-function is sandwiched between two general linear systems characterized by the reflection and transmission amplitudes r_i and t_i, $i = 1, 2$. A plane wave of amplitude E_0 incident upon the system from the right, results in a transmission amplitude E_t and a reflection amplitude E_r.

and λ' are given by the following expressions:

$$\gamma = \frac{1/(|T|^2|T_0|^2) - \mathrm{Re}^2[1/(T^*T_0)]}{|1/T_0 - 1/T|^2}, \tag{6}$$

$$\tau' = \frac{(1/|T_0|^2 - \mathrm{Re}[1/(T^*T_0)])^2}{|1/T_0 - 1/T|^2}, \tag{7}$$

$$\lambda' = \lambda |1/t_1 - r_1^*/t_1^*|^2 \, |1/T_0 - 1/T| / \sqrt{\tau'}, \tag{8}$$

where T is the *linear* transmission amplitude for the system without the δ-function at the origin ($\epsilon_0 \equiv 0$):

$$\frac{1}{T} = \frac{1}{t_1 t_2} + \frac{r_1^* r_2}{t_1^* t_2}. \tag{9}$$

Similarly, T_0 is the *linear* transmission amplitude for the case with the δ-function at the origin ($\lambda \equiv 0$),

$$\frac{1}{T_0} = \frac{1}{T} - \mathrm{i}\frac{k\epsilon_0}{2}\left(\frac{1}{t_1} - \frac{r_1^*}{t_1^*}\right)\left(\frac{1}{t_2} + \frac{r_2}{t_2}\right). \tag{10}$$

The conditions for bistability from Eq. (5) now read as

$$\frac{\gamma}{\tau'} < \frac{1}{3}, \tag{11}$$

$$\lambda' < 0, \tag{12}$$

thus, allowing bistability for positive Kerr-coefficients as well. We want to stress that the conditions for bistability depend on the transmission amplitudes of the linear systems with and without δ-function only. They can conveniently be rewritten in terms of the quantities R and θ which are defined via $1/T_0 = R\mathrm{e}^{\mathrm{i}\theta}/T$:

$$\frac{\sin^2\theta}{(R - \cos\theta)^2} \le \frac{1}{3}, \tag{13}$$

$$\mathrm{sign}(\lambda)\left(1 - \frac{\cos\theta}{R}\right) < 0. \tag{14}$$

Fig. 4 shows the phase diagram for the onset of bistability derived from Eqs. (13) and (14). Obviously, the insertion of the linear part of the nonlinear δ-function has to sufficiently alter the total transmission amplitude $1/T$ in order for bistability to occur. This alteration may be achieved by a change in the total transmission, i.e. by changing R, and/or by introducing a phase shift θ.

One can get more explicit and transparent results when the linear systems each consist of a periodic arrangement of N linear δ-functions of dielectric strength ϵ_0, and a spacing a, which is taken as the unit of length, equal to the distance between the nonlinear δ-function and the two linear systems. For low incident intensities (linear regime) this is nothing more but a Kronig–Penney δ-function model. The input vs. output relationship is now given by Eq. (5) with

$$\gamma = 1, \tag{15}$$

$$\tau' = \frac{\epsilon_0^2 k^2}{4}\frac{\sin^2(2N+1)q}{\sin^2 q}, \tag{16}$$

$$\lambda' = \lambda \frac{C^2 \sin q}{\sin(2N+1)q}, \tag{17}$$

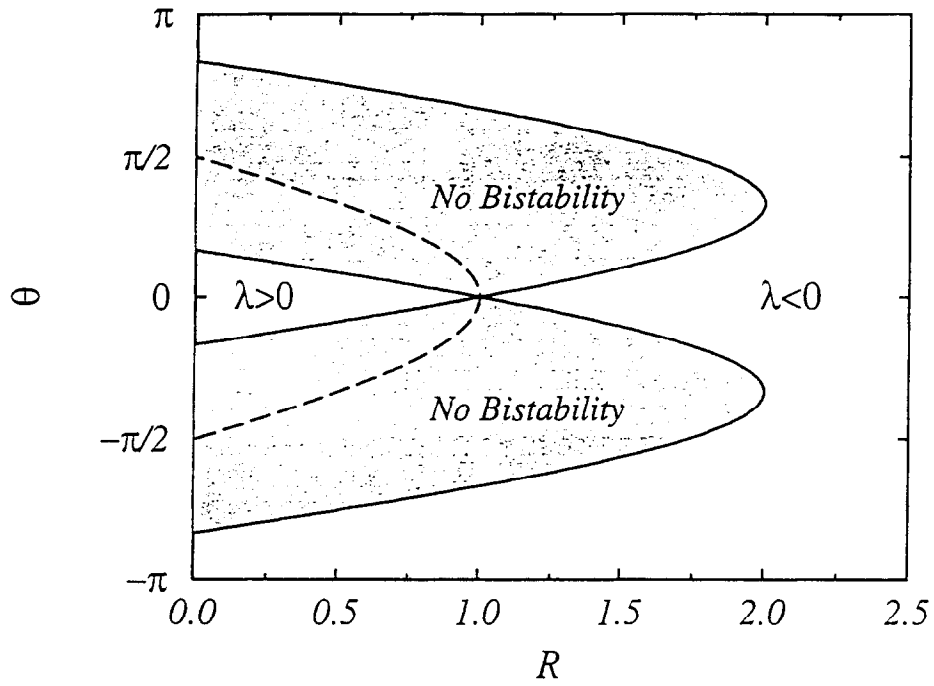

Fig. 4. The phase diagram for the onset of bistability for a δ-function sandwiched between two linear systems, as derived from Eqs. (13) and (14). θ and R are defined through $1/T_0 = Re^{i\theta}/T$ where T_0 is the total linear transmission amplitude of the two linear structures with the δ-function in the middle ($\lambda \equiv 0$) and T is the total transmission amplitude without the δ-function ($\epsilon \equiv 0$). Eq. (13) sets the values of R and θ for which we can observe bistability, outside the gray areas, while Eq. (14) (dashed line) sets the sign of the nonlinear coefficient λ for which we will observe bistability.

where

$$\cos q = \cos k - \tfrac{1}{2} k\epsilon_0 \sin k \tag{18}$$

and

$$C = 1 \mp \epsilon_0 k \sin k \frac{\sin Nq \sin(N+1)q}{\sin^2 q}. \tag{19}$$

The transmission bands of the system in the linear regime are found for $|\cos q| \leq 1$. For band gap frequencies ($|\cos q| > 1$), q should be replaced by $i|q|$ and use the lower sign in C when $\cos q < -1$.

Note that due to the renormalization of the parameters τ and λ, interesting features arise: τ' is now related to the total linear transmission coefficient of the system $\tau' = (1 - |T_{\text{Total}}|^2)/|T_{\text{Total}}|^2$, and the condition $\tau' > 3$ implies $|T_{\text{Total}}|^2 < 0.25$. Also, the constraint $\lambda < 0$ is now relaxed since it requires only $\lambda' < 0$.

In Fig. 5(a) we plot the switching-up and -down intensities of frequencies close to the first band gap. We note that the sign of λ required to obtain bistability, between successive lobes of the linear transmission curve, is alternating from $\lambda < 0$ to $\lambda > 0$. This can be understood by means of the field configuration that characterize these lobes for the linear lattice and the phase shift that is introduced to them by the nonlinear δ-function. Also, the switching intensities get smaller for frequencies closer to the band gap.

An important consequence of the introduction of the two linear systems is the presence of resonances. The phase shift introduced by the nonlinear δ-function must be enough to tune the incident wave with the shifted resonance (transmission lobe). The same transmission lobes are found in the linear transmission diagram of a finite superlattice.

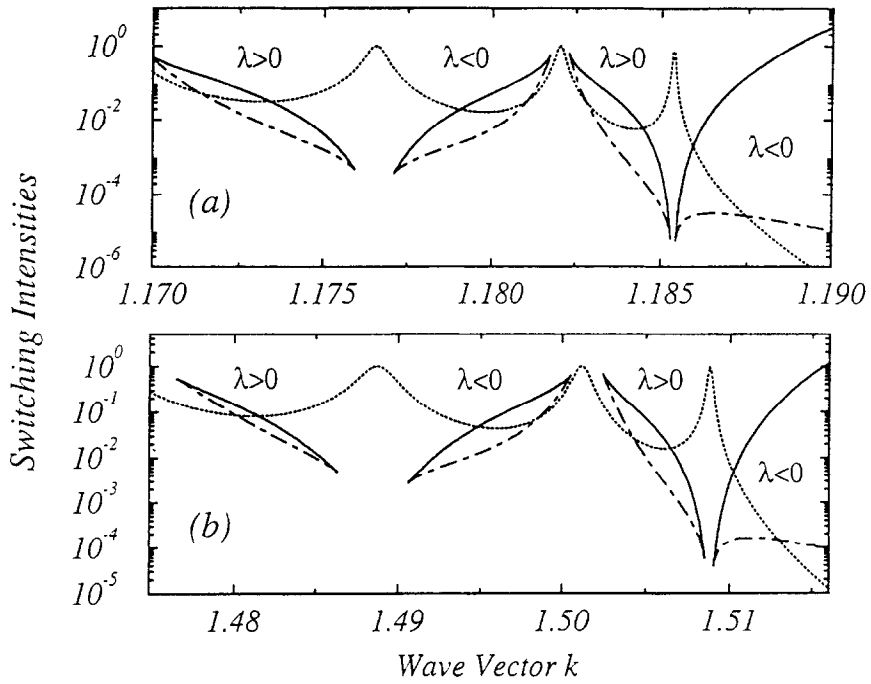

Fig. 5. Switching-up (solid line) and switching-down (dot–dashed line) intensities for a nonlinear impurity system sandwiched between two linear structures. The linear structures consist of (a) δ-functions with $N = 20$. $\epsilon_0' = \epsilon_0 = 2.5$ and spacing $a = 1$. and as a comparison. (b) a system of 41 dielectric bilayers with $d_a = d_b = 0.5$ and $n_a^2 = 1$, $n_b^2 = 5$ in analogy with the δ-function system: $d_b n_b^2 = \epsilon_0$. The b layer in the middle of the structure is nonlinear with $\epsilon_b(x) = n_b^2(1 + \lambda|E(x)|^2)$. The dotted line in both graphs is the linear transmission coefficient of the structure. The band gap starts around $k = 1.186$ for the δ-function model and $k = 1.51$ for the finite width model.

Then, from the point of view of induced phase shifts, there should be no real qualitative difference between the δ-function model and the finite layer superlattice, at least for the first bistable loop. The finite layer system differs qualitatively from the nonlinear δ-function model insofar as it always exhibits multistability (the nonlinear δ-function system is strictly bistable), a point which will be discussed in Section 3. But when considering only the first bistable loop, the very thin layer approximation may be viewed as a reliable guide to more realistic systems involving finite width nonlinear layers. This is shown in Fig. 5(b) where we plot the switching-up and -down intensities of the first bistable loop, for a finite width layered model with a finite width nonlinear impurity layer, having its system parameters defined in correspondence with the δ-function model by $\epsilon_0 = dn^2$. In order to stress the similarity, we have chosen the nonlinear layer to be equal to half-a-lattice period. We see that the δ-function model indeed captures most of the essential features of the more realistic finite width superlattice.

If the nonlinear δ-function in the middle has a linear dielectric strength $\epsilon_0' \neq \epsilon_0$ then we have to use the renormalizations

$$\tau' \to \tau' a^2, \tag{20}$$

$$\lambda' \to \lambda' \frac{\epsilon_0'}{\epsilon_0} a^{-1}, \tag{21}$$

where

$$a = 1 + \frac{\epsilon_0' - \epsilon_0}{\epsilon_0} \frac{C \sin q}{\sin(2N+1)q}. \tag{22}$$

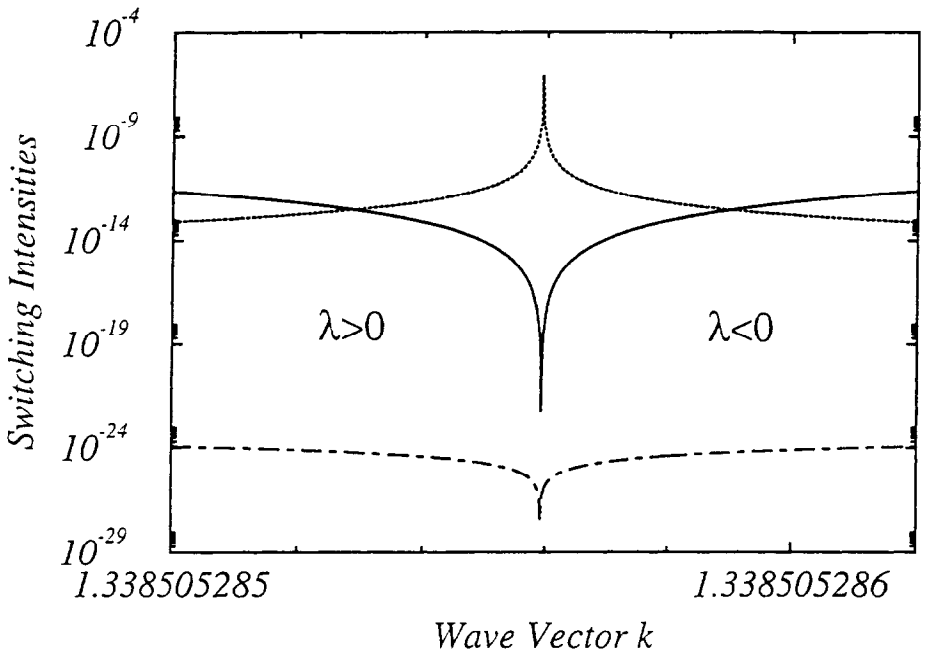

Fig. 6. The switchig intensities (solid and dot–dashed lines for switching-up and -down, respectively) for the same system of Fig. 5(a) for the δ model but now for the impurity case $\epsilon_0' = 1$. The linear impurity mode is deep in the gap (dotted line corresponds to the linear transmission coefficient). Note that for frequencies very close to this mode the switching intensities become extremely small.

Similar behavior is then obtained for this impurity case, for frequencies inside the transmission band, for both systems. However, for band gap frequencies, and for $\epsilon_0' > \epsilon_0$, no gap impurity mode exists in the δ-function model so the response of the two systems inside the gap is different. For $\epsilon_0' < \epsilon_0$, both systems exhibit an impurity mode inside every band gap [14]. When the fields are turned on, a positive nonlinearity in the middle of the structure will shift the impurity mode to lower frequencies, while a negative nonlinearity will shift it to higher frequencies. As a consequence, when $\lambda > 0$ bistability is observed at frequencies lower than that of the linear impurity mode, while for $\lambda < 0$ we must use higher frequencies.

The switching-up and -down intensities are generally $Y_- \sim 1/|\lambda'|$ and $Y_+ \sim \tau'/|\lambda'|$, and for band gap frequencies it is generally $\tau' \gg \lambda' \gg 1$, yielding extremely low switching-down intensities and extremely high switching-up intensities. Nevertheless, for frequencies extremely close to the linear defect frequency, it is $\lambda' \gg \tau' \gg 1$, yielding extremely small switching-up intensities as well. As can be seen in Fig. 6, where we plot the switching intensities for a large impurity (linear impurity mode deep inside the band gap), the order of magnitude for an $N = 20$ system is well below 10^{-20}, and becomes exponentially small as N gets larger. To get a feeling for this number, assume that typical electronic nonlinearities are of the order of $|\lambda| \sim 10^{-15}\,\mathrm{cm}^2/\mathrm{W}$. Then $Y_\pm \sim 10^{-5}\,\mathrm{W/cm}^2$. Furthermore, the intensity at the nonlinear defect layer is small enough, to secure that the nonlinearity is well described as a Kerr nonlinearity: The nonlinear effect does not saturate and the nonlinear layer will not get damaged from intense fields. However, the price, one has to pay to achieve low power thresholds, is to maintain extreme accuracy in the incident frequency, due to the extremely high Q of the mode. For the system described in Fig. 6 this accuracy is of the order of $\Delta k/k \sim 10^{-10}$. This is quite unrealistic. This ratio gets exponentially small for increasing N. Thus, for a realistic application it is the laser's line-width which determines the power thresholds for bistability and in general compromise has to be found.

3. Dielectric superlattice with nonlinear impurity: Resonance states

In Section 2, we have investigated the response of a very thin layer of nonlinear material sandwiched between two linear Bragg-reflector structures. We demonstrated that such a structure can exhibit bistability with very low switching threshold as a result of coupling to the impurity mode in the stop gap of the linear structure. In this section, we consider the situation when the nonlinear layer is not thin. There are qualitative differences between the response of a nonlinear finite width layer and a nonlinear δ-function layer. We have seen that a single finite width dielectric layer exhibits bistability for both positive and negative Kerr-coefficients (Fig. 2(a)), whereas the single nonlinear δ-function exhibits bistability for negative Kerr-coefficient only. Similarly and in contrast to the strictly bistable δ-function model, dielectric superlattices with a nonlinear impurity always exhibit multistability. This, we will show, has to do with the fact that impurity modes exist for each value of $\Delta\epsilon$. We can understand all these properties qualitatively if we view the finite nonlinear layer as consisting of a sequence of nonlinear δ-functions. Then resonance phenomena allow to bypass the limited behaviour of a single nonlinear δ-function. However, multistability is much harder to detect than bistability, because the field values at the nonlinear layer may be very large and oscillating.

Let us first investigate the localized mode solution for a finite width nonlinear layer sandwiched between two Bragg-reflectors. The nonlinear wave equation inside the impurity layer is given by

$$\frac{\mathrm{d}}{\mathrm{d}x^2}E(x) + k_0^2(1 + \lambda|E(x)|^2)E(x) = 0, \tag{23}$$

where $k_0 = n^2(\omega/c)$. This equation may be solved by means of the following ansatz [6]:

$$E(x) = E_0 g(x)\mathrm{e}^{\mathrm{i}\phi(x)}. \tag{24}$$

Inserting this ansatz into Eq. (23) leads to a separation of the amplitude and phase function, $g(x)$ and $\phi(x)$, respectively:

$$\frac{\mathrm{d}}{\mathrm{d}x}\phi(x) = \frac{W}{g^2(x)}, \tag{25}$$

$$\left(\frac{\mathrm{d}g(x)}{\mathrm{d}x}\right) + \frac{W}{g^2(x)} + k_0^2 g^2(x) + \frac{1}{2}\tilde{\lambda}k_0^2 g^4(x) = A, \tag{26}$$

where $\tilde{\lambda} = \lambda|E_0|^2$ is the effective nonlinearity, and A and W are constants to be determined. Upon introducing $I(x) = g^2(x)$, the solution may be cast in the deceptively simple form:

$$\int_{I(x_0)}^{I(x)} \mathrm{d}I \frac{1}{(AI - k^2I^2 - \tilde{\lambda}k^2I^3/2 - W^2)^{1/2}} = \pm 2(x - x_0), \tag{27}$$

$$\phi(x) = \phi(x_0) + W\int_{x_0}^{x} \mathrm{d}x' \frac{1}{I(x')}. \tag{28}$$

The four unknowns A, W, $\phi(x_0)$, $I(x_0) \equiv g^2(x_0)$ have to be determined from the boundary conditions at x_0. In particular, W is related to the energy flux through the layer as can be seen evaluating the Poynting "vector" $S = -c^2/8\pi\omega\,\mathrm{Re}[\mathrm{i}E^*(x)(\mathrm{d}E(x)/\mathrm{d}x)] = c^2|E_0|^2W/8\pi c$. In the case of $\lambda = 0$ it is an easy exercise to obtain the linear solutions from Eq. (27). For $\lambda \neq 0$, despite the apparent simplicity of Eq. (27), a closed form solution cannot be obtained in general. The reason for this difficulty is seen as follows: The solution of Eq. (27) comes down to

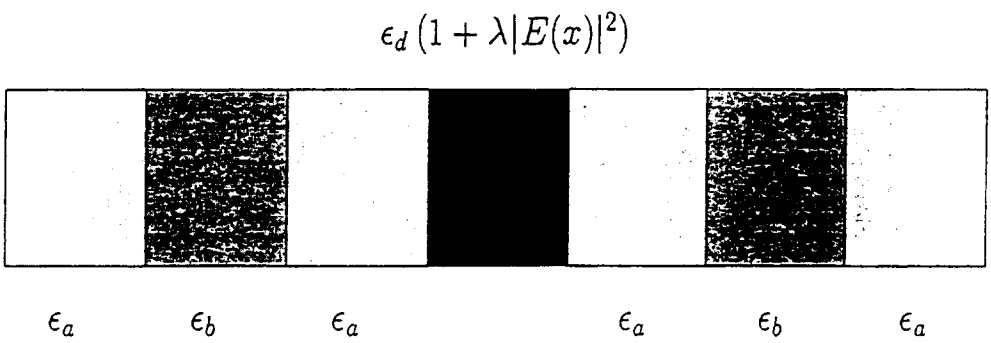

Fig. 7. The model superlattice used in this section. A nonlinear layer of dielectric constant $\epsilon_d(1+\lambda|E(x)|^2)$ and thickness l centered at $x=0$ is sandwiched between two infinitely extended superlattices of alternating layers with dielectric constants ϵ_a and ϵ_b, and widths a and $a-d$, respectively.

finding the roots of the denominator, where A and W depend on the boundary values in a complicated way. This task can be accomplished in two special circumstances only: If $\mathrm{d}\phi(x_0)/\mathrm{d}x=0$, then, according to Eq. (25) we already have one root, leaving us with the simple exercise of solving a quadratic equation. Similarly, $W=0$ immediately gives the root $I=0$, again reducing the problem to a quadratic equation. The first case was exploited by Chen and Mills [6] in solving the transmission problem through a single finite width nonlinear layer only, without the superlattices on both sides.

We, however, are interested in the second situation. Apparently, $W=0$ implies $S=0$. This corresponds to a spatially symmetric situation, i.e., a situation where parity is a good "quantum" number. Speaking in terms of the transmission experiment we have in mind, this amounts for solving for the stationary or resonance states for which input equals output. This distinction is of no importance in the linear problem, because there we can construct any state by an appropriate superposition of stationary states. Obviously, this cannot be done in a nonlinear problem. Consider now the case where the nonlinear layer, centered at $x=0$, is sandwiched between two infinitely extended linear superlattices of alternating layers of dielectric constants ϵ_a and ϵ_b as well as widths $a-d$ and d, respectively (cf. Fig. 7): Since the stationary states have parity $p=\pm 1$, we may impose the following values of the E-field $E(0)$ and its derivative $E'(0)$ at the origin:

Even solution ($p=1$):

$$E(0)=E_0\neq 0 \quad\Rightarrow\quad \phi(0)=0,\ g(0)=1, \qquad E'(0)=0 \quad\Rightarrow\quad g'(0)=0.$$

Odd solution ($p=-1$):

$$E(0)=0 \quad\Rightarrow\quad \phi(0)=W=0,\ g(0)=0,$$
$$E'(0)=E_0k_0\sqrt{1+\tilde{\lambda}/2}\neq 0 \quad\Rightarrow\quad g'(0)=k_0\sqrt{1+\tilde{\lambda}/2}.$$

Here, we have chosen the nonzero values of the field's derivative for the odd solution in a particular convenient form, so that for both parities A is given by $A=k_0^2(1+\tilde{\lambda}/2)$.

To compare with numerical studies, the above equations define the value of E_0 and, thus, the effective nonlinearity $\tilde{\lambda}$. Consequently, for a given frequency we need to search for the symmetric states (resonant states) in the transmission problem and compute the field E_0 at the origin. For given λ we then get the effective nonlinearity $\tilde{\lambda}=\lambda|E_0|^2$.

The solution $I(x)$ will depend on both the parity and the sign of one of the roots, which depends on the sign of $\tilde{\lambda}$ [19], and is going to be expressed in terms of Jacobian elliptic functions [21].

Outside the nonlinear layer the waves obey the Block–Floquet theorem. We employ the "travelling wave" description [20], which decomposes the field $E(x)$ and (implicitly) its derivative $E'(x)$ into left and right moving waves:

$$\boldsymbol{E}(x) = \begin{pmatrix} A_r e^{ikr} \\ A_l e^{-ikx} \end{pmatrix}. \tag{29}$$

Within this formalism, the Block–Floquet theory for a defect state inside the photonic band gap created by the linear superlattice reads as (connecting the fields in the middle of one linear A-layer at $x = s$ to the fields at $x = a + s$, where a is a lattice constant):

$$(\mathcal{M} \pm e^{-\gamma a}\mathcal{E})\boldsymbol{E}(s) = 0, \tag{30}$$

where the matrix elements of $\mathcal{M}$ are well-known:

$$\mathcal{M}_{11} = e^{ika(a-d)}\left(\cos(k_b d) + \frac{1}{2}i\left(\frac{k_b}{k_a} + \frac{k_a}{k_b}\right)\sin(k_b d)\right), \qquad \mathcal{M}_{12} = \frac{1}{2}i\left(\frac{k_b}{k_a} - \frac{k_a}{k_b}\right)\sin(k_a d),$$

where $k_a = (\omega/c)\sqrt{\epsilon_a}$, $k_b = (\omega/c)\sqrt{\epsilon_b}$ and $\mathcal{M}_{11} = \mathcal{M}_{22}^*$, $\mathcal{M}_{12} = \mathcal{M}_{21}^*$. Inside the nonlinear layer we know the field and its derivative at the origin. Using the solutions inside the nonlinear layer, we calculate the field at the interface to the A-material, translate (field and derivative are continuous at the boundary!) the results into the travelling wave formalism and propagate them to the middle of the A-layer, i.e. we obtain $\boldsymbol{E}(s)$:

$$(\boldsymbol{E})_1(s) = e^{ik_a s}\sqrt{I(l/2)} - \frac{i}{k_a}e^{ik_a s}\frac{d}{dx}\sqrt{I(l/2)}, \tag{31}$$

$$(\boldsymbol{E})_2(s) = ((\boldsymbol{E})_1(s))^*, \tag{32}$$

where $s = (a - l)/2$ and l is the thickness of the nonlinear layer. Thus, (30) constitutes two linear equations, the second being the complex conjugate of the first. Upon separating this complex equation into real and imaginary part, we observe that the real part does not contain γ and may thus be used to determine ω:

$$\sin(k_a(a-d))\cos(k_b d) + \frac{1}{2}\left(\frac{k_b}{k_a} + \frac{k_a}{k_b}\right)\cos(k_a(a-d))\sin(k_b d) + \frac{1}{2}\left(\frac{k_b}{k_a} - \frac{k_a}{k_b}\right)\sin(k_b d)\psi(\omega) = 0, \tag{33}$$

where $\psi(\omega)$ contains the information about the nonlinear layer. Define

$$\chi^{(0)}(x) = \frac{\sqrt{I(x)}}{k_a}\frac{d\left(\sqrt{I(x)}\right)}{dx}, \qquad \chi^{(+/-)}(x) = I(x) \pm \frac{1}{k_a^2}\left(\frac{d\left(\sqrt{I(x)}\right)}{dx}\right)^2.$$

Then $\psi(\omega)$ is given as

$$\psi(\omega) = \frac{\cos(k_a s)\chi^{(-)}(l/2) + 2\sin(k_a s)\chi^{(0)}(l/2)}{\chi^{(+)}(l/2)}, \tag{34}$$

where $s = a - d + l$ (a = lattice constant; d = thickness of the B layers; l = thickness of the nonlinear layer). $\sqrt{I(l/2)}$ and $d(\sqrt{I(l/2)})/dx$ have to be evaluated according to the sign of $\tilde{\lambda}$ and parity. Eqs. (33) and (34) define the solution for an impurity mode for our structure. These impurity modes manifest themselves as resonances in the nonlinear multistable response, for frequencies inside the gap of the linear superlattice. In the δ-function model we had one such resonance, as required from its strictly bistable character. For practical applications, the linear superlattices cannot be infinitely extended. However, as long as the number of the layers is large enough to have a well-defined localized solution, the resonant frequencies should be given exactly by Eq. (33).

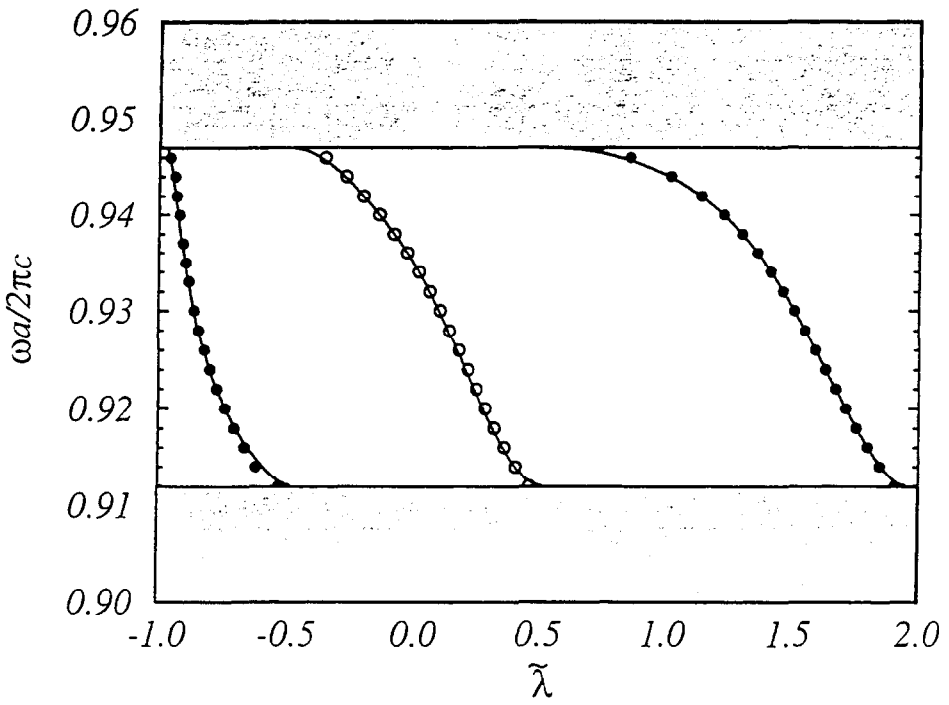

Fig. 8. The resonance state frequencies as a function of the effective nonlinearity $\tilde{\lambda}$ inside the third band gap. The linear superlattice consists of equal thickness layers of alternating dielectric constants $\epsilon_a = 1$ and $\epsilon_b = 5$, while the nonlinear layer has $\epsilon_d = 8$, $l = d$ and $\lambda = 1$. Solid lines correspond to the analytical results while circles correspond to the results of numerical simulation using 20 bilayers on each side of the nonlinear layer. Filled circles correspond to states with even parity, while open circles correspond to states with odd parity. The gray areas correspond to parts of the third and the fourth transmission bands.

Fig. 8 shows the resonance state frequencies as a function of $\tilde{\lambda}$ for a linear superlattice consisting of equally wide layers of alternating dielectric constant $\epsilon_a = 1$ and $\epsilon_b = 5$. The nonlinear layer is described by $n^2 = 8$, $l = d$ and $\lambda = 1$. Solid lines represent the analytical solution according to Eq. (33), while the circles correspond to the results of numerical simulations using 20 bilayers on each side of the nonlinear layer. In addition, the parity of the resonance states is indicated. Evidently, the agreement between the two methods is excellent, thus illustrating the multistable behavior.

4. Nonlinear dielectric superlattice

In Sections 2 and 3 we have investigated the response of linear superlattices with a nonlinear impurity. We have seen how the modulated band gap impurity mode is responsible for the bistable and/or multistable response of the superlattice. We now consider the case when the structure consists of alternating layers of two dielectric materials, one of which has an intensity-dependent Kerr nonlinearity, $\epsilon = \epsilon_0 + \alpha_2|E|^2$. The global transmission diagrams of such multilayer structures with a Kerr nonlinearity were investigated within a Kronig–Penney δ-function model [17]. It was found that the effectiveness of the nonlinearity is strongly modified by the frequency. In addition the nonlinear responses of the positive and the negative nonlinear media are distinctly different due to the modulation of the dispersion relation by the superlattice. Many dominant features were understood through the analysis of stable periodic orbits of the corresponding nonlinear mapping as well as the analysis of various spectrum and

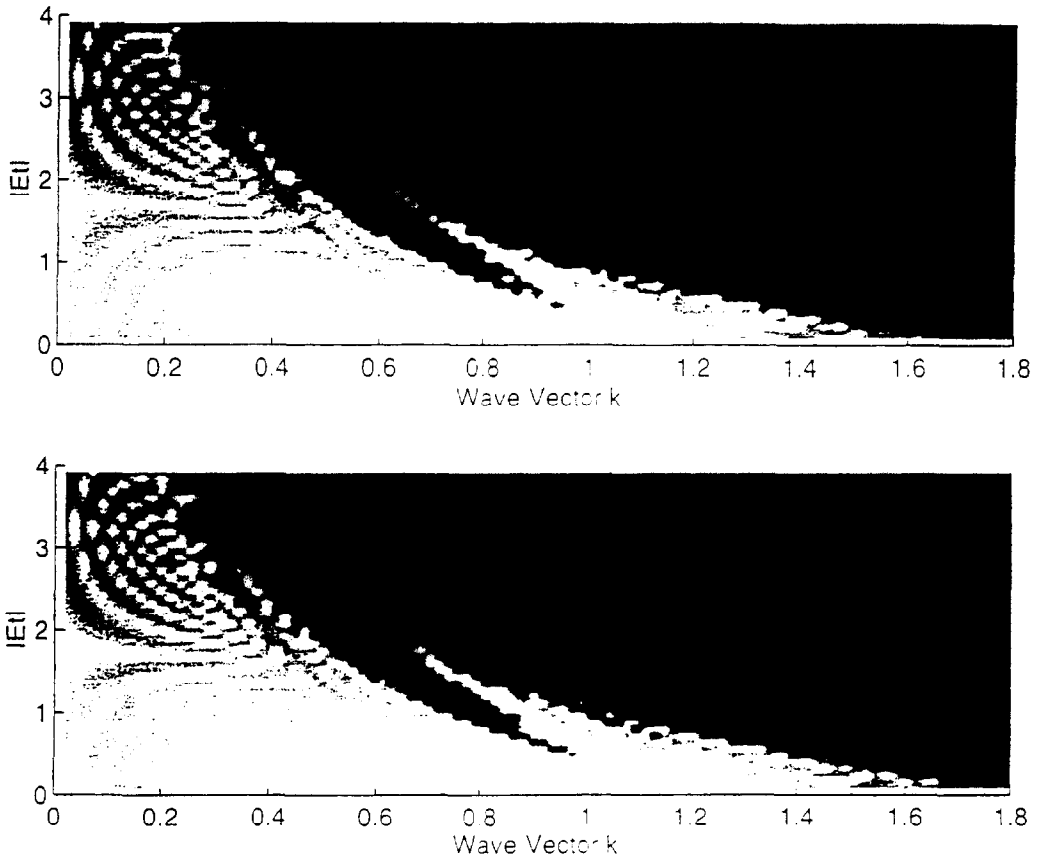

Fig. 9. The transmission diagram for a nonlinear superlattice of $L = 80$ units with a positive Kerr-coefficient: (a) δ-function model with $\alpha = 1$ and (b) exact solutions with linear layers of thickness 0.9, $\epsilon = 1$, and nonlinear layers of thickness 0.1 and $\epsilon_0 = 10$. Higher bands (not shown) show similar behavior.

stability bounds of the nonlinear difference and the corresponding differential equations. A simple and intuitive picture of the formation of gap solitons and soliton trains, based on a mechanical analogy, was also presented. These understandings may prove useful for incorporating nonlinearity in systems of higher dimensions, e.g., in photonic band gap structures [13].

All these results were based on the Kronig–Penney δ-function model. Such a model offers the advantage of being amenable for some analytical treatment and is expected to work well when the nonlinear layer is thin compared with the wavelength of the incident wave. In this section we will investigate its general adequacy as well as its limitations by comparing the results derived from the Kronig–Penney δ-function model with direct numerical solutions of wave propagation in nonlinear superlattice of finite thickness.

The formulation of the steady state plane wave transmission problem in nonlinear superlattices has been described in detail elsewhere [17]. The structure consists of alternating layers of two dielectric materials, one of which has an intensity-dependent Kerr nonlinearity, $\epsilon = \epsilon_0 + \alpha_2|E|^2$. For normal incidence of a plane wave, the electric field amplitude $E(x)$ satisfies the equation

$$\frac{\mathrm{d}^2E(x)}{\mathrm{d}x^2} + \frac{\omega^2}{c^2}\epsilon(x)E(x) = 0, \tag{35}$$

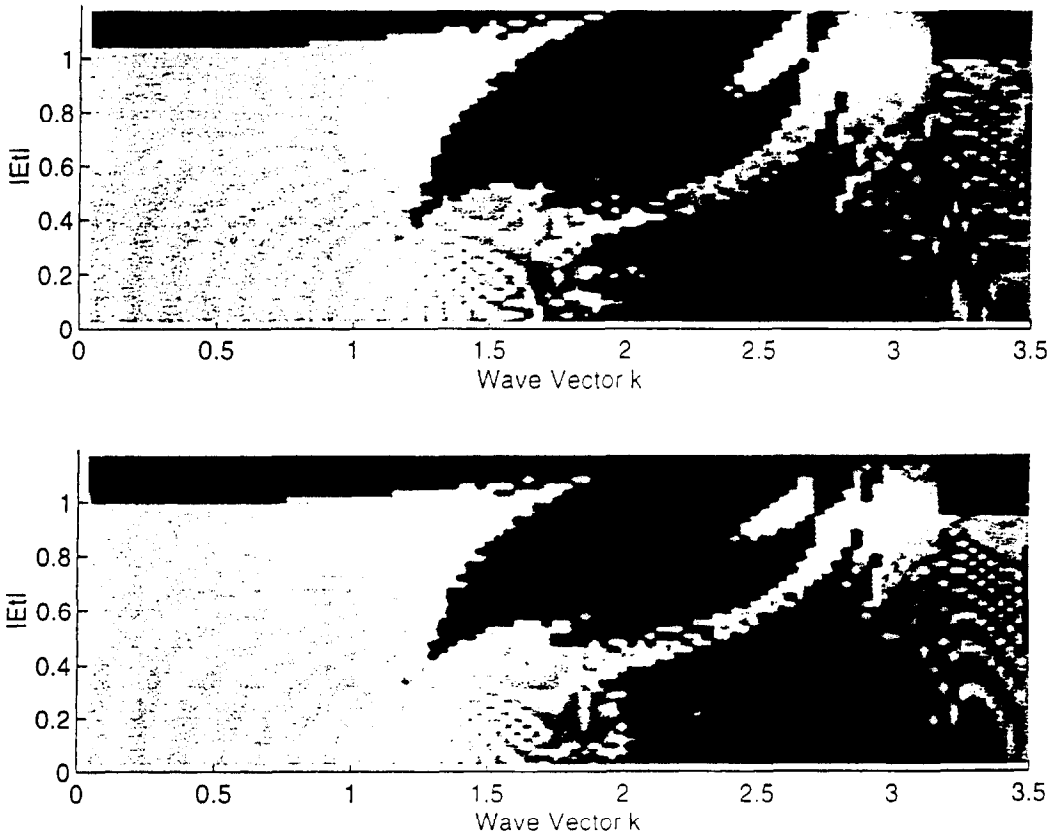

Fig. 10. The transmission diagram for a nonlinear superlattice of $L = 80$ units with a negative Kerr-coefficient: (a) δ-function model with $\alpha = 1$; (b) linear layers of thickness 0.9, $\epsilon = 1$ and nonlinear layers of thickness 0.1 and $\epsilon_0 = 10$.

where ω is the optical frequency, and c is the vacuum speed of the light. $\epsilon(x)$ is the dielectric constant which varies along the structure and depends on the local field intensity at nonlinear layers. The transmission characteristics are obtained by solving Eq. (35) under the boundary condition

$$E(x,t) = \begin{cases} E_0 e^{ikx} + E_r e^{-ikx} & \text{for } x < 0, \\ E_t e^{ikx} & \text{for } x > L, \end{cases} \tag{36}$$

where E_0, E_t, and E_r are the amplitude of the incident, transmitted, and reflected waves, respectively. Wave vector $k = \omega/c$, and L is the total length of the structure. The transmission coefficient T is defined as $T = |E_t|^2/|E_0|^2$.

Eq. (35) can be solved [6] by matching at the layer interfaces the analytical solutions in each nonlinear layer, which may be expressed in terms of the Jacobi elliptic functions [6]. A much simpler numerical approach, however, is to first discretize the structure and then iterate the difference equation numerically across the sample, starting from the output field E_t. Our numerical results are obtained this way.

The Kronig–Penney δ-function model, on the other hand, describes a system with infinitesimally thin nonlinear layers [17]. In this model, the electric field obeys

$$\frac{d^2E(x)}{dx^2} + \frac{\alpha\omega^2}{c^2}\sum_{n=1}^{N}(1 + \lambda|E(x)|^2)E(x)\delta(x-n) + k^2E(x) = 0. \tag{37}$$

This can be easily rewritten [17] as a difference equation in terms of the field at the nonlinear layers, E_n.

$$E_{n+1} + E_{n-1} + (2\cos k - \alpha k \sin k(1 + \lambda|E_n|^2))E_n, \tag{38}$$

where $\alpha = \epsilon_0 a$ and $\lambda = \alpha_2/\alpha$. a is the thickness of the nonlinear layers. We have assumed that the linear medium is a vacuum ($\epsilon = 1$), and the distance between the neighboring nonlinear layers, $d = a + b$, is taken as one unit length. The δ-function model can be viewed as an approximation when the nonlinear layer is thin compared with the effective wavelength within it.

In order to compare the results obtained for the δ-function model with the results obtained for the finite width nonlinear layers, we have solved numerically the wave equation (Eq. (35)) for a system with nonlinear layers of width 0.1 unit length and linear layers ($\epsilon = 1$) of width 0.9 unit length. The global transmission diagrams in the k–E_t plane for the positive Kerr-coefficient is shown in Fig. 9(b) as a grey scale plot, along with the results from the δ-function model (Fig. 9(a)). The general features are remarkably similar. Good agreement is also obtained when the Kerr nonlinear coefficient is negative (Fig. 10). These transmission diagrams show features that have been understood through analysis of stable periodic orbits and various spectrum and stability bounds [17].

A remarkable phenomenon occurred in the nonlinear response of superlattice structures is the existence of localized gap soliton solutions in the stop band of the linear regime [6]. In the previous study [17] with the δ-function model, only in the negative Kerr media did we find gap soliton solutions. This is in disaggreement with the conclusion of Chen and Mills [6] that soliton solutions exist regardless of the sign of the nonlinearity. In Fig. 11, we

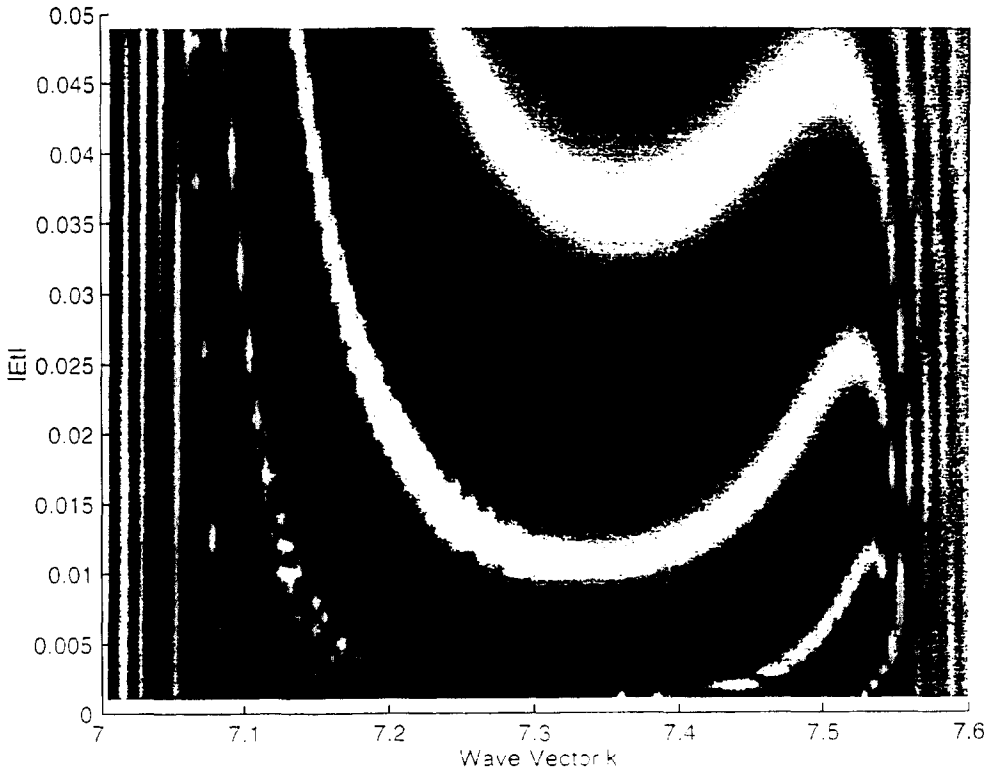

Fig. 11. The resonant transmission trajectories of single and multiple solitons in the third stop-band of a nonlinear finite thickness superlattice of $L = 80$ units with a positive Kerr-coefficient. Linear layers of thickness 0.9, $\epsilon = 1$, and nonlinear layers of thickness 0.1 and $\epsilon_0 = 16$.

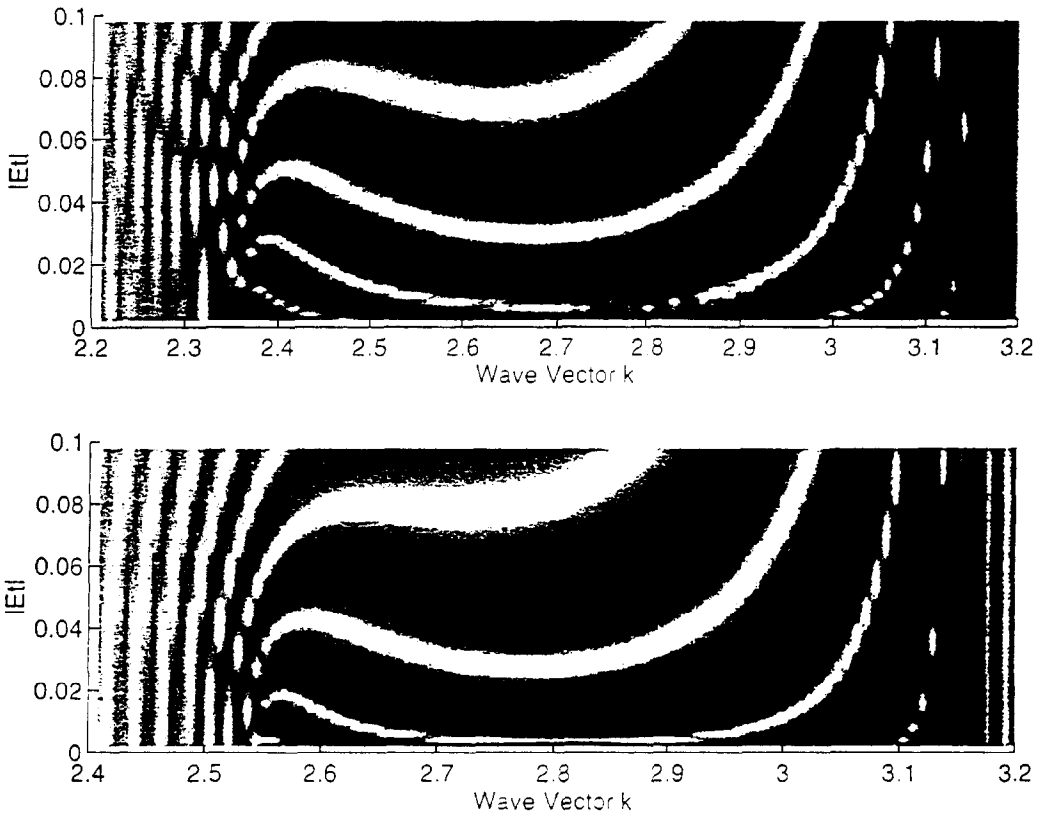

Fig. 12. The resonant transmission trajectories of single and multiple solitons in the first stop-band of an $L = 80$ multilayer system with a negative Kerr-coefficient: (a) δ-function model with $\alpha = 0.35$; (b) finite thickness bilayers with linear layers of thickness 0.9, $\epsilon = 1$ and nonlinear layers of thickness 0.1 and $\epsilon_0 = 3.5$.

show the transmission diagram within the stop band for a finite width superlattice with a positive nonlinear coefficient. Clearly, resonant trajectories exist. Examination of the solutions show well-localized waves symmetrically distributed at the center of the structure. Different resonance bands correspond to solutions containing different number of solitons, analogous to the situation with negative nonlinearity. Here, the inadequacy of the δ-function model shows up, by not giving soliton solutions in the gap. For negative nonlinear coefficient, the transmission diagram of the superlattice structure again is in good agreement with that of the δ-function model (see Fig. 12).

To understand why the δ-function model fails to describe the formation of gap soliton in superlattices with positive nonlinear coefficient, we have to examine the physical mechanism in which gap solitons form when nonlinearity is incorporated in the model. This was elucidated with a mechanical analogy in the previous work [17]. The soliton forms only when the frequency is in the forbidden region of the spectrum in a linear system, i.e., in the gap. As the wave intensity varies along the structure, the dielectric constant of the nonlinear layers changes accordingly. Consequently the location of the effective transmission bands moves. For the soliton to form, the linearized transmission band has to shift in the right direction such that the incident frequency merges into it. This is illustrated in Fig. 13 in which we show a single soliton profile (Fig. 13(a)) in the stop band. The corresponding effective transmission band edges are shown in Fig. 13(b), calculated from the linear dispersion relation using the local dielectric constant. Clearly, as the soliton intensity increases, the effective transmission band shifts towards the incident frequency and eventually takes it completely in the vicinity of the center of the soliton.

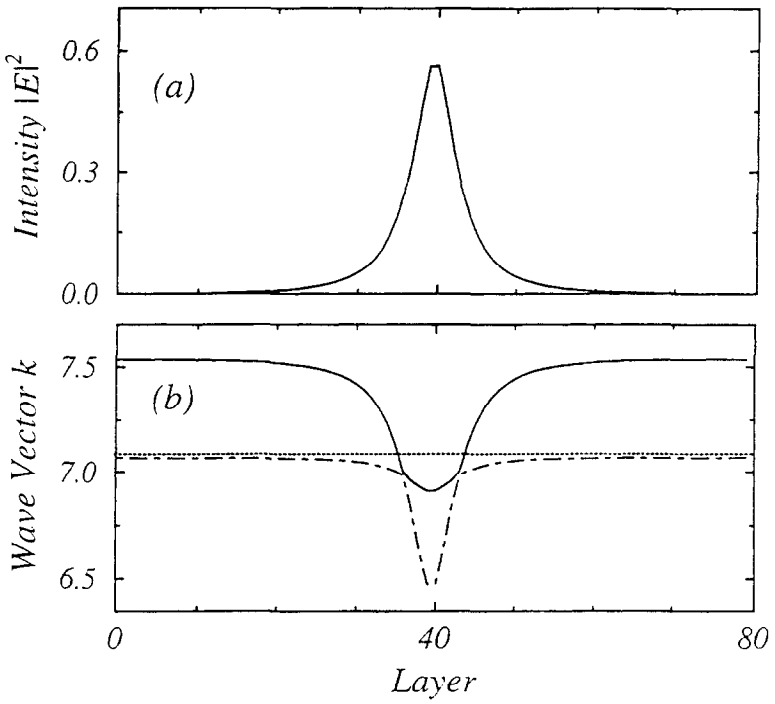

Fig. 13. Illustration of gap soliton formation in a system with $L = 80$ layers with positive nonlinearity. Linear layers of thickness 0.9, $\epsilon = 1$, and nonlinear layers of thickness 0.1 and $\epsilon_0 = 16$. $k = 7.07369$ and $E_l = 0.01$: (a) profile of a gap soliton and (b) the local effective stop-band edges as determined from the soliton profile. The stop-band extends from the dashed line (low frequency stop-band edge) to the solid line (high frequency stop-band edge). The thin line is the incident frequency. Clearly, the incident frequency merges inside the effective transmission band around the center of the solition.

Examination of the effective transmission bands as a function of the effective dielectric constant in the nonlinear layers shows clearly the difference between the δ-function model and the more realistic multilayer system (Fig. 14). For the negative nonlinearity (the portion below the dotted line), the collapse of the gap is described well with the δ-function (Fig. 14(a)). But for positive nonlinearity (the portion above the dotted line), the shift of bottom of the bands towards lower frequency in the real system is completely missed in the δ-function. This is not surprising, since the bottom of the band in the δ-function model is always located at $k = m\pi$. Thus, the rigidness of the band edge in the δ-function model prevents the frequency below the bottom of the band from merging into the effectve transmission band when the field intensity increases and therefore hinders the formation of gap solitons.

We have also investigated systems with thicker nonlinear layers and found qualitatively similar behavior. Quantitative agreement of course worsens as the nonlinear layer thickness increases. However, the essential features remain the same. Thus the δ-function model seems to be sufficiently adequate for a qualitative study of nonlinear response to radiation.

5. Conclusions

We have investigated the general problem of electromagnetic wave propagation through a one-dimensional system consisting of a nonlinear layer sandwiched between two linear superlattices. We provide a general frame on which calculations can be done, based on the transmission characteristics of the linear layers. In the case of a very thin layer.

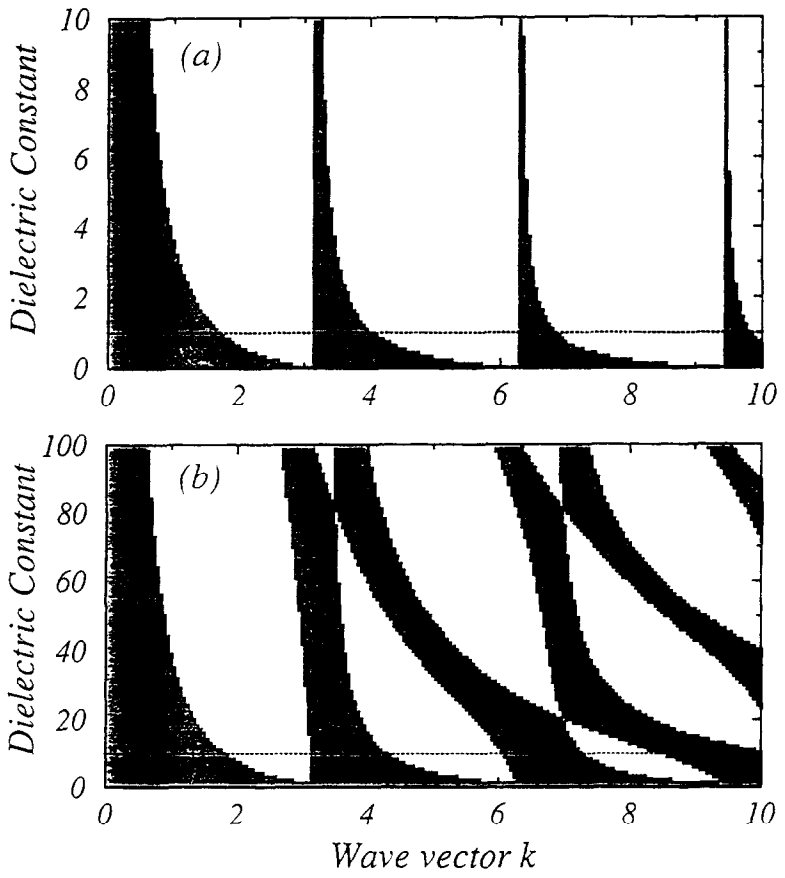

Fig. 14. The transmission band as a function of the effective dielectric constant at the nonlinear layers, $L = 80$: (a) δ-function model with $\alpha = 1$; (b) linear layers of thickness 0.9, $\epsilon = 1$ and nonlinear layers of thickness 0.1 and $\epsilon_0 = 10$. The horizontal line indicates the bands in the linear regime.

we have shown that a δ-function approximation is adequate. A cubic equation is derived, describing the nonlinear bistable response, with normalized parameters that characterize the experimental situation. We obtain bistability in the gap of the linear system, via the impurity mode, and find that the switching thresholds can be made extremely small by enlarging the structure and/or widening the gap. An analytical solution for the localized resonance modes in the band gap is obtained for the finite width nonlinear layer problem. Multistability, the basic feature absent in the δ-function model, is now obtained. Finally, we have examined many aspects of the nonlinear response in multilayer structures and found the δ-function model quite adequate, aside from the obvious deficiency of processing a rigid bottom band edge. The model captures the most essential features in the transmission characteristics and therefore should be widely used due to its simplicity.

Acknowledgements

Ames Laboratory is operated for the US Department of Energy by Iowa State University under Contract No. W-7405-Eng-82. This work was supported by the Director for Energy Research office of Basic Energy Sciences and Advanced Energy Projects and by NATO Grant No. 940647.

References

[1] H.G. Winfull, J.H. Marburger, E. Garmire, Appl. Phys. Lett. 35 (1979) 379.
[2] W. Chen, D.L. Mills, Phys. Rev. B 35 (1987) 524.
[3] H.M. Gibbs, S.L. McCall, T.N.C. Venkatesan, Phys. Lett. 36 (1976) 1135.
[4] B. Xu, N.B. Ming, Phys. Rev. Lett. 71 (1993) 3959.
[5] C.J. Herbert, W.S. Capinski, M.S. Malcuit, Opt. Lett. 17 (1992) 1037.
[6] W. Chen, D.L. Mills, Phys. Rev. B 36 (1987) 6269.
[7] F.S. Felber, J.H. Marburger, Appl. Phys. Lett. 28 (1976) 731.
[8] M. Okuda, K. Onaka, Jpn. J. Appl. Phys. 16 (1977) 769.
[9] F. Deylon, Y. Levy, B. Souillard, Phys. Lett. 57 (1986) 2010.
[10] Y. Wan, C.M. Soukoulis, Phys. Rev. B 41 (1990) 800.
[11] D. Hennig, H. Gabriel, G.P. Tsironis, M. Molina, Appl. Phys. Lett. 64 (1994) 2934.
[12] M.I. Molina, G.P Tsironis, Int. J. Modern Phys. B 9 (1995) 1899.
[13] C.M. Soukoulis (Ed.), Photonic Band Gap Materials, Kluwer Academic Publisher, Dordrecht, 1996.
[14] D.R. Smith et al., J. Opt. Soc. Am. B 10 (1993) 314.
[15] W. Chen, D.L. Mills, Phys. Rev. Lett. 58 (1987) 160.
[16] C. Martine De Sterke, J. Sipe, in: E. Wolf (Ed.), Progress in Optics, vol. 33, Elsevier, Amsterdam, 1994.
[17] Q.Li, C.T. Chan, K.M. Ho, C.M. Soukoulis, Phys. Rev. B 53 (1996) 15 577.
[18] E. Lidorikis, Q. Li, C.M. Soukoulis, Phys. Rev. B 54 (1996) 10 249.
[19] P.F. Byrd, M.D. Friedman, Handbook of Elliptic Intergrals for Engineers and Scientists, Springer, Berlin, 1971.
[20] K. Busch, C.T. Chan, C.M. Soukoulis, NATO ASI, Series E 315 (1996) 465.
[21] E. Lidorikis, K. Busch, Q. Li, C.T. Chan, C.M. Soukoulis, to be published.